Appl. Math. Mech. -Engl. Ed.
DOI 10.1007/s10483-015-1958-9

Applied Mathematics and Mechanics (English Edition)

Surface effects on mechanical behavior of elastic nanoporous materials under high strain*

Zixing LU†, Fan XIE, Qiang LIU, Zhenyu YANG

School of Aeronautics Science and Engineering, Beihang University, Beijing 100191, China

Abstract This paper studies surface effects on the mechanical behavior of nanoporous materials under high strains with an improved anisotropic Kelvin model. The stress-strain relations are derived by the theories of Euler-Bernoulli beam and surface elasticity. Meanwhile, the influence of strut (or ligament) size on the mechanical properties of nanoporous materials is discussed, which becomes a key factor with consideration of the residual surface stress and the surface elasticity. The results show that the decrease in the strut diameter and the increase in the residual surface stress or the surface elasticity can both lead to an increase in the carrying capacity of nanoporous materials. Furthermore, mechanical behaviors of anisotropic nanoporous materials in different directions (the rise direction and the transverse direction) are investigated. The results indicate that the surface effects in the transverse direction are more obvious than those in the rise direction for anisotropic nanoporous materials. In addition, the present results can be reduced to the cases of conventional foams as the strut size increases to micron-scale, which confirms validity of the model to a certain extent.

Key words surface effect, nanoporous, anisotropy, high strain

Chinese Library Classification O343.5, O341
2010 Mathematics Subject Classification 70A65

1 Introduction

In recent years, nanoporous materials have attracted extensive attention for their novel mechanical properties and their potential applications in microelectrode array chip[1], molecular fluids[2], photocatalysis[3], gas or molecular abruption[4], catalysis[5], energy absorption[6], electric conduction[7], sensor[8], actuation[9], etc. Due to the large amount of surface, nanoporous materials exhibit unique mechanical behaviors, which have been confirmed to be size-dependent in experiments[10–13]. Biener et al.[11] found that nanoporous gold could be as strong as bulk Au, despite being a highly porous material, and the ligaments in nanoporous gold approached the theoretical yield strength of Au. Hodge et al.[12] believed that the foam strength was governed by the ligament size at the nanoscale, in addition to the relative density. Weissmüller et al.[14] found that the relation among the strain, the surface stress, and the elastic parameters depended strongly on the geometry of the microstructure.

* Received Jun. 17, 2014 / Revised Nov. 13, 2014
Project supported by the National Natural Science Foundation of China (Nos. 11472025, 10932001, and 11272030)
† Corresponding author, E-mail: luzixing@buaa.edu.cn

Up to now, the theory of surface elasticity proposed by Gurtin and Murdoch[15] has been extensively used to reveal the size-dependent mechanical properties of nanoporous materials[16]. Based on the theory, Feng et al.[17] investigated the surface effects on the elastic properties of nanoporous materials using the cubic unit cell model. Lu et al.[18] arrived at a similar conclusion as that of Feng et al.[17] using the Kelvin model. Further, Xia et al.[19] used a modified Timoshenko beam model to study the elastic microstructural buckling behavior of nanoporous materials, which exhibited a significant dependence on the average ligament width. Goudarzi et al.[20] and Moshtaghin et al.[21] obtained a macroscopic size-dependent yield function for nanoporous materials by considering the residual surface stress and the surface elasticity. The aforementioned works indicate that the surface elasticity plays a significant role in the elastic properties of nanoporous materials while the residual surface stress contributes more to the buckling strength and the yield strength.

The theory of surface elasticity proposed by Gurtin and Murdoch[15] has also been used to investigate the high elastic deformation of nanostructured materials, which has been observed in experiments[22–24]. Based on the theory, Liu et al.[25] established the governing equations of large displacement for nanowires with different boundary conditions. It showed that the fixed-fixed nanobeam would get "stiffer" under the positive residual surface stress, and vice versa, "softer" under the negative one. Wang and Yang[26] studied the influence of surface stresses on the postbuckling behavior of nanowires. Wang et al.[27] presented a nonlinear rod model to investigate the surface effects of the superelasticity of nanohelices. Again, the above works verify that the theory of surface elasticity is well adequate to describe the large elastic deformation behaviors of nanostructured materials. To the best of our knowledge, the large elastic deformation behaviors of nanowires or nanohelices have been extensively studied, while the similar work on nanoporous materials is scarce.

Moreover, the microstructural anisotropy of nanoporous materials was observed in the experiments[28], which would have influence on the high deformation on the macro-level. To reveal the influence of structural anisotropy, Lu et al.[29–30] developed an anisotropic Kelvin model to analyze the mechanical properties of anisotropic open-cell elastic foams without surface effects. However, few papers have been published to study the mechanical properties of anisotropic nanoporous materials under high elastic deformation.

The main object of the present work is to analyze the surface effects of anisotropic nanoporous materials under high elastic deformation. Based on our previous work[18,29–30], this paper studies the high strain behaviors of elastic nanoporous materials using the Kelvin model, whilst the influence of structural anisotropy is also considered. First, by an improved anisotropic Kelvin model, the analytical strain-stress relation is deduced for the nanoporous materials under high strains of both compression and tension. Then, the surface effects on the nonlinear response are investigated. Finally, the influence of structural anisotropy on the overall response is discussed.

2 Theoretical description and derivation

2.1 Surface stress-strain relationship

As we know, surface atoms experience different local environments from bulk atoms[16]. Based on the previous work[31], the surface stress tensor τ_{ij} can be expressed as follows:

$$\tau_{ij} = \gamma\delta_{ij} + \frac{\partial\gamma}{\partial\varepsilon_{ij}}, \tag{1}$$

where γ is the free energy per unit area, ε_{ij} is the strain tensor, and δ_{ij} is the Kronecker delta. Further, Lu et al.[18] and Feng et al.[17] developed a nanobeam model, which consisted of bulk and surface with zero thickness. The isotropic surface layer and the isotropic bulk of the material are supposed. Further, the uniform thickness t_0 and Young's modulus E_1 of the surface

layer are also assumed. Consequently, a surface constitutive relation for the one-dimensional form of Eq. (1) can be expressed as[32]

$$\tau = \tau_0 + E_{\mathrm{s}}\varepsilon_{\mathrm{s}}, \tag{2}$$

where τ is the surface stress, τ_0 is the residual surface stress, $E_{\mathrm{s}} = E_1 t_0$ is the surface elastic modulus, and ε_{s} is the surface strain. A mathematical description of the transverse stresses induced from longitudinal stresses of the tortuous surfaces is given by the generalized Young-Laplace equation as follows[33–34]:

$$\Delta\sigma_{ij} n_i n_j = \tau_{\alpha\beta}\kappa_{\alpha\beta}, \tag{3}$$

where $\Delta\sigma_{ij}$ is the stress jump across a surface, n_i is the unit normal vector, and $\kappa_{\alpha\beta}$ is the curvature tensor.

2.2 Anisotropic Kelvin model

Nanoporous materials have sponge-like structures with open-cell network structures, which consist of interconnected nano-ligaments. As shown in Fig. 1(a), an improved Kelvin model with a surface layer and a uniform circular cross-section, which has a periodical structure in the three-dimensional space, is developed. The anisotropic Kelvin model consists of eight hexagons and six quadrilaterals, in which the inclination angle β denotes the orientation of the oblique ligament relative to the rise direction, and λ is the anisotropy ratio defined as $\lambda = \tan\beta$, as shown in Fig. 1(b). When $\beta = \pi/4$, the model is reduced to the classic Kelvin model. Similar to the analyzed method of Lu et al.[18], a simplified periodical structural cell under compression (under tension only changing in the loading direction) is extracted, as shown in Fig. 2.

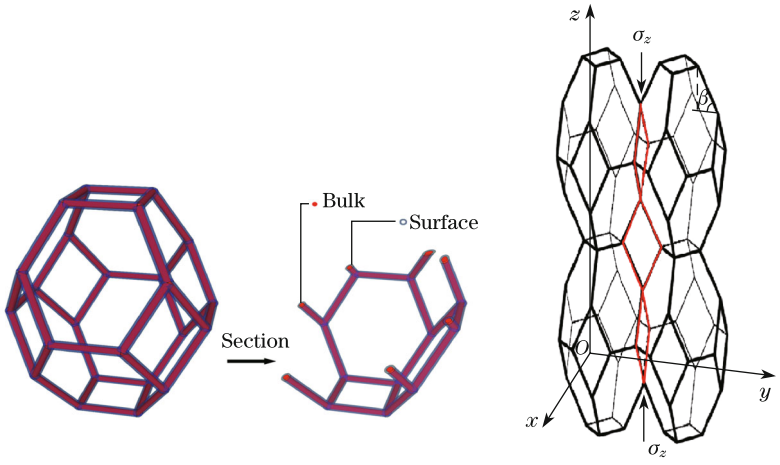

(a) Schematic (b) Four cells

Fig. 1 Anisotropic Kelvin model with surface layer

2.3 Loading in rise direction

As shown in Fig. 3, a curvilinear coordinate system (s, θ) with the origin O located in the midpoint of strut AE is introduced to analyze the deformation of the half-strut. The coordinate s is the measurement of strut length, and the coordinate θ is the angle between the tangent to the strut and the rise direction.

Just as shown in Fig. 3, a transverse distributed force is applied on the strut bending. Based on the results of Wang and Feng[35], the distributed transverse force can be expressed as

$$p(s) = H\frac{\mathrm{d}\theta}{\mathrm{d}s}, \tag{4}$$

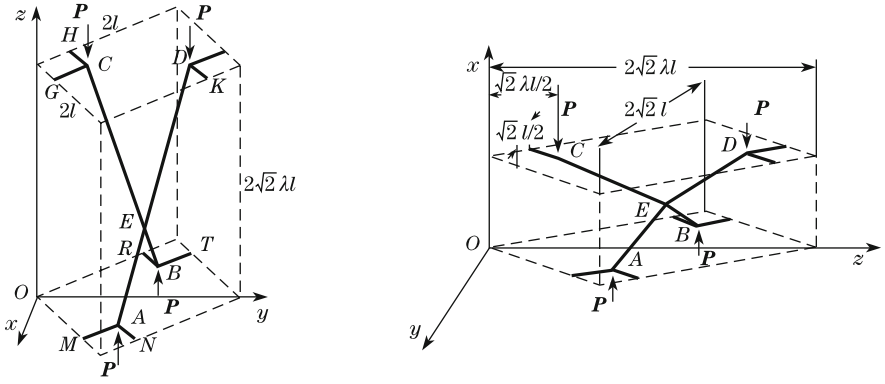

(a) Loading in rise direction (b) Loading in transverse direction

Fig. 2 Periodical model under compression

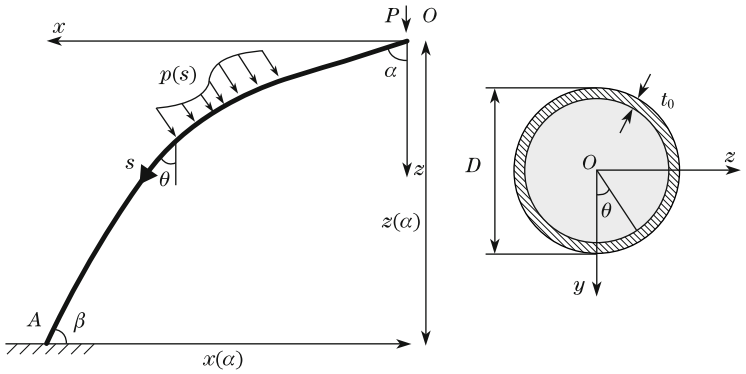

Fig. 3 Half-strut element OA with surface layer under compression

where H is determined by the cross-sectional shape of the strut and the surface stress. This study assumes that the cross-section of the strut is a circle. Thus, the expression of H is[18]

$$H = 2\int_{-\pi/2}^{\pi/2} \frac{D\tau\cos\theta}{2}\mathrm{d}\theta = 2\tau D, \tag{5}$$

where D is the diameter of the strut. Although the vertical displacement of the strut is big enough, the strain is still in the infinitesimal range, as mentioned in Ref. [25]. Substituting Eqs. (2) and (5) into Eq. (4) and considering the small deformation approximation, i.e., $\varepsilon_{\mathrm{s}} \approx -\frac{D}{2}\frac{\mathrm{d}\theta}{\mathrm{d}s}$, we have

$$p(s) = H\frac{\mathrm{d}\theta}{\mathrm{d}s} = 2\Big(\tau_0 - \frac{D}{2}E_{\mathrm{s}}\frac{\mathrm{d}\theta}{\mathrm{d}s}\Big)D\frac{\mathrm{d}\theta}{\mathrm{d}s} \approx 2\tau_0 D\frac{\mathrm{d}\theta}{\mathrm{d}s} = H_0\frac{\mathrm{d}\theta}{\mathrm{d}s}, \tag{6}$$

where the component of $(\frac{\mathrm{d}\theta}{\mathrm{d}s})^2$ is neglected. The effective bending rigidity of the composite beam is defined as follows:

$$(EI)^* = \frac{\pi E_0 D^4}{64} + \frac{\pi E_{\mathrm{s}} D^3}{8}, \tag{7}$$

where E_0 denotes Young's modulus of the bulk material.

The moment at a common position is

$$M = -Px - \int_0^s p(t)\left(\sin\theta(t)(x(s) - x(t)) + \cos\theta(t)\left(z(s) - z\left(t\right)\right)\right)\mathrm{d}t, \tag{8}$$

where x represents a variable in the x-coordinate in Fig. 3, and t is an integral variable. According to the knowledge of materials mechanics, the differential equation of the deflection curve is as follows:

$$(EI)^*\frac{\mathrm{d}\theta}{\mathrm{d}s} = -Px - \int_0^s p(t)(\sin\theta(t)\left(x(s) - x(t)\right) + \cos\theta(t)\left(z(s) - z(t)\right))\mathrm{d}t. \tag{9}$$

Based on the geometric relationship shown in Fig. 3,

$$\frac{\mathrm{d}x}{\mathrm{d}s} = \sin\theta, \quad \frac{\mathrm{d}z}{\mathrm{d}s} = \cos\theta. \tag{10}$$

Differentiating Eq. (9) with respect to s, we have

$$(EI)^*\frac{\mathrm{d}^2\theta}{\mathrm{d}s^2} = -P\sin\theta - H_0\sin(\theta - \alpha). \tag{11}$$

When $H_0 = 0$ in Eq. (11) and $E_\mathrm{s} = 0$ in Eq. (7), it will be reduced to the form without the surface effects in Ref. [29], similar hereinafter. Multiplying Eq. (11) with $\mathrm{d}\theta$ and integrating from the point O yield

$$\frac{(EI)^*}{2}\Big(\frac{\mathrm{d}\theta}{\mathrm{d}s}\Big)^2 = P\left(\cos\theta - \cos\alpha\right) + H_0(\cos(\theta - \alpha) - 1). \tag{12}$$

Equation (12) can also be expressed as

$$\mathrm{d}s = (2P\left(\cos\theta - \cos\alpha\right)/(EI)^* + 2H_0\left(\cos(\theta - \alpha) - 1\right)/(EI)^*)^{-1/2}\mathrm{d}\theta. \tag{13}$$

The length of the half-strut OA in Fig. 3 is l', which can be expressed as

$$l' = \frac{\sqrt{2}l\sqrt{\lambda^2 + 1}}{4}. \tag{14}$$

The integrating equation (13) gives

$$l' = \int_{\frac{\pi}{2}-\beta}^{\alpha}(2P\left(\cos\theta - \cos\alpha\right)/(EI)^* + 2H_0\left(\cos(\theta - \alpha) - 1\right)/(EI)^*)^{-1/2}\mathrm{d}\theta, \tag{15}$$

where β denotes the inclination angle at the point A.

Clearly, P is a function of variable α. Then, the stress in the z-direction σ_z can be expressed as

$$\sigma_z = \frac{P(\alpha)}{2l^2}. \tag{16}$$

Based on Eq. (10),

$$\mathrm{d}z = \cos\theta\mathrm{d}s. \tag{17}$$

Integrating Eq. (17) gives the length of the projection length of OA in the z-direction, which is

$$z(\alpha) = \int_{\frac{\pi}{2}-\beta}^{\alpha}\cos\theta(2P(\cos\theta - \cos\alpha)/(EI)^* + 2H_0(\cos(\theta - \alpha) - 1)/(EI)^*)^{-1/2}\mathrm{d}\theta. \tag{18}$$

The initial projection length of OA in the z-direction is $\sqrt{2}\lambda l/4$. Hence, the strain is given as

$$\varepsilon_z = (\sqrt{2}\lambda l/4 - z(\alpha))/(\sqrt{2}\lambda l/4) = 1 - \frac{4z(\alpha)}{\sqrt{2}\lambda l}. \tag{19}$$

In conclusion, the compressive stress-strain relationship in the z-direction can be evaluated from Eqs. (16) and (19) by a given value of λ. Similarly, under tension, Eqs. (18) and (19) can be expressed as

$$z(\alpha) = \int_{\frac{\pi}{2}-\beta}^{\alpha} \cos\theta(2P(\cos\alpha - \cos\theta)/(EI)^* + 2H_0(1-\cos(\theta-\alpha))/(EI)^*)^{-1/2}\mathrm{d}\theta, \tag{20}$$

$$\varepsilon_z = \frac{4z(\alpha)}{\sqrt{2}\lambda l} - 1. \tag{21}$$

Under tension, the stress in the z-direction σ_z can also be expressed as Eq. (16). The tensile stress-strain curve in the z-direction can be obtained from Eqs. (16) and (21) under tension.

2.4 Loading in transverse direction

In Fig. 4, the deformation of OC is displayed with O located in the midpoint of the strut EC. Similarly, the differential equation of the deflection curve yields

$$(EI)^*\frac{\mathrm{d}\theta}{\mathrm{d}s} = -Pz - \int_0^s p(t)(\sin\theta(t)(z(s)-z(t)) + \cos\theta(t)(x(s)-x(t)))\mathrm{d}t. \tag{22}$$

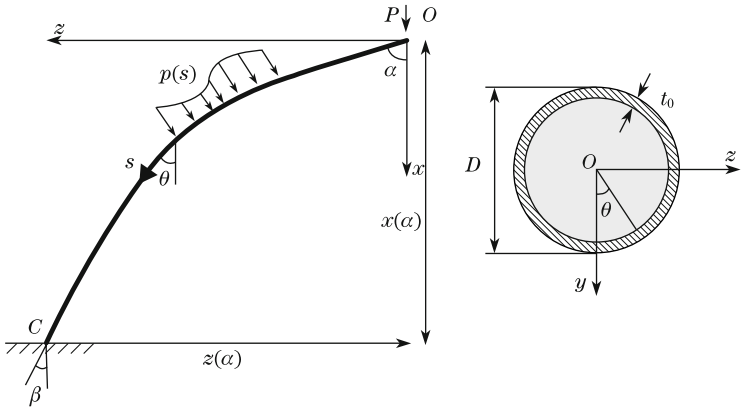

Fig. 4 Half-strut element OC with surface layer under compression

In Fig. 4, we have

$$\frac{\mathrm{d}z}{\mathrm{d}s} = \sin\theta, \quad \frac{\mathrm{d}x}{\mathrm{d}s} = \cos\theta. \tag{23}$$

Similarly, combining Eqs. (22) and (23) yields

$$\mathrm{d}s = (2P(\cos\theta - \cos\alpha)/(EI)^* + 2H_0(\cos(\theta-\alpha)-1)/(EI)^*)^{-1/2}\mathrm{d}\theta. \tag{24}$$

The length l' is similarly written as

$$l' = \int_\beta^\alpha (2P(\cos\theta - \cos\alpha)/(EI)^* + 2H_0(\cos(\theta-\alpha)-1)/(EI)^*)^{-1/2}\mathrm{d}\theta. \tag{25}$$

The imposed stress σ_x to the model can be expressed as

$$\sigma_x = \frac{P(\alpha)}{2\lambda l^2}. \tag{26}$$

Similarly, the length of the deformed strut in the x-direction is

$$\begin{aligned} x(\alpha) = & 2\int_{\beta}^{\alpha} \cos\theta(2P(\cos\theta - \cos\alpha)/(EI)^* + 2H_0(\cos(\theta-\alpha)-1)/(EI)^*)^{-1/2}\mathrm{d}\theta \\ & + 2\int_{\pi/4}^{\alpha} \cos\theta(2P(\cos\theta - \cos\alpha)/(EI)^* + 2H_0(\cos(\theta-\alpha)-1)/(EI)^*)^{-1/2}\mathrm{d}\theta. \end{aligned} \tag{27}$$

In Fig. 2(b), the initial length of the strut in the x-direction is $\sqrt{2}l$. Then, the strain is

$$\varepsilon_x = 1 - \frac{x(\alpha)}{\sqrt{2}l}. \tag{28}$$

Hence, the stress-strain relationship in the transverse direction can be evaluated by combination of Eqs. (26) and (28). Similarly, under tension, Eqs. (27) and (28) can be expressed as follows:

$$\begin{aligned} x(\alpha) = & 2\int_{\beta}^{\alpha} \cos\theta(2P(\cos\alpha - \cos\theta)/(EI)^* + 2H_0(1-\cos(\theta-\alpha))/(EI)^*)^{-1/2}\mathrm{d}\theta \\ & + 2\int_{\pi/4}^{\alpha} \cos\theta(2P(\cos\alpha - \cos\theta)/(EI)^* + 2H_0(1-\cos(\theta-\alpha))/(EI)^*)^{-1/2}\mathrm{d}\theta, \end{aligned} \tag{29}$$

$$\varepsilon_x = \frac{x(\alpha)}{\sqrt{2}l} - 1. \tag{30}$$

Under tension, the stress in the x-direction σ_x can also be expressed as Eq. (26). The stress-strain curve in the x-direction can be obtained from Eqs. (26) and (30) under tension.

It is noteworthy that the present derivation can be reduced to those of Lu et al.[29–30] which have been proved by the finite element method when the surface effect is not considered. Furthermore, the present model is consistent with the form of Zhu et al.[36] when λ is specified as 1. Moreover, Young's modulus of Lu et al.[18] can be obtained by the present results by taking limit.

3 Examples and discussion

In this paper, the parameters of nanoporous materials are selected as follows[27]: the bulk Young's modulus is $E_0 = 70.29$ GPa, the residual surface stress is $\tau_0 = 0.91$ N/m, and the surface elastic modulus is $E_\mathrm{s} = 5.19$ N/m. In addition, we take the relative density of nanoporous materials as 0.07 in the following discussion. To facilitate the analysis, two parameters are defined for convenience of comparison of the results. The dimensionless stress is adopted according to Lu et al.[37], i.e.,

$$\overline{\sigma} = \sigma/(E_0(\rho/\rho_0)^2), \tag{31}$$

where E_0 denotes Young's modulus of the bulk material, and ρ and ρ_0 are the densities of the nanoporous material and the bulk material, respectively. To highlight the surface effects, the normalized stress is defined as the ratio of stress of nanoporous materials to that of macroporous materials with the same relative density, i.e.,

$$\sigma^* = \sigma_\mathrm{n}/\sigma_\mathrm{m}, \tag{32}$$

where σ_{n} is the stress of nanoporous materials, and σ_{m} is the stress of macro-porous materials. The following results are calculated by the MATLAB software.

Figure 5 illustrates the dimensionless stress-strain curves obtained from the isotropic nanoporous materials ($\lambda = 1$) with different strut diameters, in which $\tau_0 = 0.91$ N/m and $E_{\mathrm{s}} = 5.19$ N/m. To conduct a direct comparison, the results of macro-porous materials derived by Zhu et al.[36] and Lu et al.[30] are also presented. Figure 5 shows that the dimensionless stress of nanoporous materials increases nonlinearly with the strain, and the increasing rate becomes smaller for larger compressive strain, while the increasing rate becomes larger for larger tensile strain. It is observed that the tension/compression asymmetry is very significant on account of geometric nonlinearity under high strains. The curves dramatically rise up as the strut diameter decreases, indicating that the mechanical behavior of nanoporous materials is size-dependent under high strains of both compression and tension. Moreover, the initial slope of stress-strain curve also increases as the strut diameter decreases, which is in accord with those in the work of Feng et al.[17] and Lu et al.[29]. However, such surface effects would not disappear until the strut diameter D is larger than 50 nm, and then the stress-strain curve of nanoporous materials approaches that of macro-porous materials.

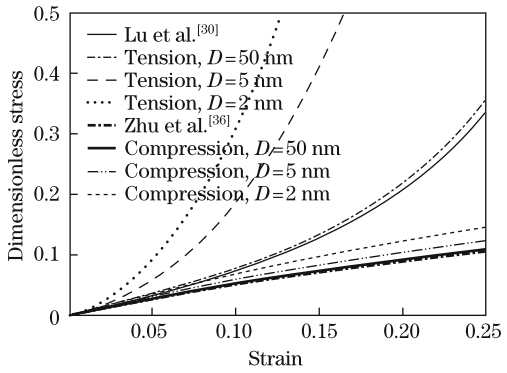

Fig. 5 Dimensionless stress-strain curves of isotropic nanoporous materials with different strut diameters ($\lambda = 1$, $\tau_0 = 0.91$ N/m, and $E_{\mathrm{s}} = 5.19$ N/m)

The surface effects of nanoporous materials are similar under compression and tension. For the sake of brevity, we only present the compressive results for convenience. In Fig. 6(a), the variation of dimensionless compressive stress-strain curves with surface elasticity is presented for isotropic nanoporous materials, $\tau_0 = 0.91$ N/m. As the surface elasticity increases, the initial stiffness of nanoporous materials evidently increases, and the compressive curves rise up as well. It indicates that the surface elasticity has a significant effect on the high strain behaviors of nanoporous materials. Especially, the influence of surface elasticity on compressive behavior becomes more evident as the strain increases. For nanoporous materials with $E_{\mathrm{s}} = 0$, its compressive behavior is close to that of macro-porous materials.

The influence of the residual surface stress τ_0 on the dimensionless compressive stress-strain curves of nanoporous materials is shown in Fig. 6(b), where $\lambda = 1$ and $E_{\mathrm{s}} = 5.19$ N/m. The strain-stress curve with a positive residual surface stress is higher than that with $\tau_0 = 0$, while the curve with a negative residual surface stress is lower than that with $\tau_0 = 0$. Especially, the strain-stress curve is even lower than that of macro-porous materials when the negative residual surface stress is low enough. Similarly, the influence of residual surface stress on compressive behavior becomes more distinct with the increase in the strain. This phenomenon is consistent with the work of Liu et al.[25].

From the above discussion, the surface effects of nanoporous materials are determined by the combined effects of the surface elasticity and the residual surface stress. Moreover, under

high strains, both of them have significant influence on the mechanical behaviors of nanoporous materials.

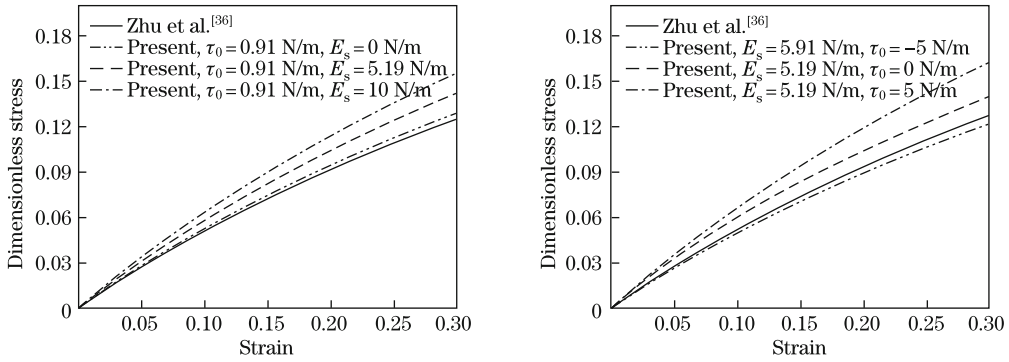

(a) Effect of surface elasticity (b) Effect of residual surface stress

Fig. 6 Dimensionless compressive stress-strain curves of isotropic nanoporous materials with 5 nm diameter

To reveal the influence of structural anisotropy, the compressive strain-stress curves of anisotropic nanoporous materials are shown in Fig. 7, and our previous works are presented[29]. The compressive stress-strain curves rise up and go down in the rise and transverse directions, respectively. The variation tendency of mechanical properties for nanoporous materials is similar to that of macro-porous materials, which was provided by Lu et al.[29]. Furthermore, the curves dramatically rise up as the strut diameter decreases in different directions, which have a similar tendency with isotropic nanoporous materials. Moreover, it is obviously shown that the isotropic curve with $D=2$ nm of nanoporous materials is even higher than the anisotropic curve of macro-porous materials in the rise direction. Hence, both the strut size and the anisotropy have a great effect on the mechanical behaviors of nanoporous materials. The carrying capacity of the nanoporous materials can be enhanced by decreasing the strut diameter or increasing the anisotropy ratio.

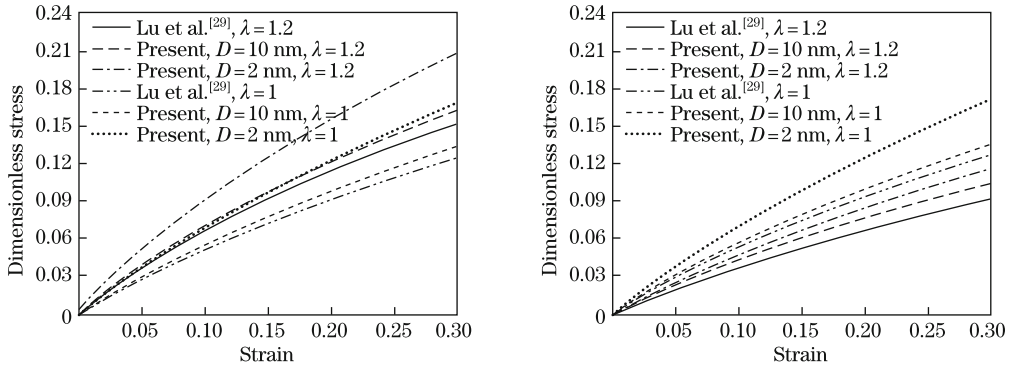

(a) In rise direction (b) In transverse direction

Fig. 7 Dimensionless compressive stress-strain curves of anisotropic nanoporous materials with different strut diameters ($\tau_0 = 0.91$ N/m and $E_s = 5.19$ N/m)

To facilitate comparison, the compressive stress is also expressed as the form of normalized stress (see Eq. (32)) as shown in Fig. 8. It shows that the normalized stress in the transverse direction is higher than that of isotropic nanoporous materials, while the normalized stress in the

rise direction is lower. It indicates that the structural anisotropy would affect the surface effects of nanoporous materials, which are enhanced in the transverse direction but is weakened in the rise direction. The reason is that the angle between the strut axis (e.g., the line CE in Fig. 2(a)) and the transverse direction is larger than that between the strut axis and the rise direction, and thus the bending deformation of strut is more significant for transverse compression. Interestingly, the distance between the isotropic curve and the one of the transverse direction is larger than that between the isotropic curve and the one of the rise direction, indicating that the surface effects are reinforced in the transverse direction for anisotropic nanoporous materials. In addition, it is shown that the normalized stress of transverse direction increases more rapidly with the strain than that of the isotropic compression and that of the rise direction. In other words, the enhancement of surface effects with increasing strains is more remarkable in the transverse direction for anisotropic nanoporous materials.

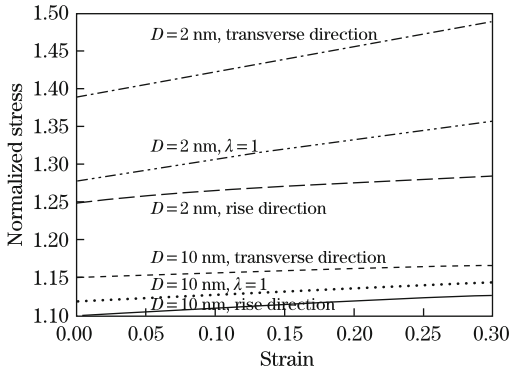

Fig. 8 Normalized compressive stress-strain curves of anisotropic nanoporous materials with different strut diameters in two directions ($\tau_0 = 0.91$ N/m and $E_s = 5.19$ N/m)

Combining Fig. 7 with Fig. 8, we can conclude that the surface effects in the transverse direction would be reinforced while the surface effects in the rise direction would be weakened for anisotropic nanoporous materials.

4 Conclusions

Based on an improved anisotropic Kelvin model, we use the theories of Euler-Bernoulli beam and surface elasticity to derive the stress-strain relationships under high strains of both compression and tension for elastic nanoporous materials. This work studies the effect of strut size on the mechanical behaviors of nanoporous materials, in which the residual surface stress and surface elasticity are incorporated. The dimensionless stress-strain curves nonlinearly rise up as the strut diameter decreases and the surface elasticity increases. The residual surface stress would lead to an increase in the carrying capacity of nanoporous materials. For anisotropic nanoporous materials, the surface effects in the transverse direction would be reinforced, while the surface effects in the rise direction would be weakened.

References

[1] Wesche, M., Hüske, M., Yakushenko, A., Bruggemann, D., Mayer, D., Offenhausser, A., and Wolfrum, B. A nanoporous alumina microelectrode array for functional cell-chip coupling. *Nanotechnology*, **23**(49), 495303 (2012)

[2] Arakcheev, V. G. and Morozov, V. B. *Vibrational Spectra of Molecular Fluids in Nanopores*, IOP Publishing, Bristol (2012)

[3] Yang, X., Lian, X. J., Liu, S. J., Wang, G., Jiang, C. P., Tian, J., Chen, J. W., and Wang, R. L. Enhanced photocatalytic performance: a β-Bi_2O_3 thin film by nanoporous surface. *Journal of Physics D*: *Applied Physics*, **46**(3), 35103 (2013)

[4] Meynen, V., Cool, P., and Vansant, E. F. Verified syntheses of mesoporous materials. *Microporous and Mesoporous Materials*, **125**(3), 170–223 (2009)

[5] Silvestre-Albero, J., Serrano-Ruiz, J. C., Sepúlveda-Escribano, A., and Rodríguez-Reinoso, F. Zn-modified MCM-41 as support for Pt catalysts. *Applied Catalysis A*: *General*, **351**(1), 16–23 (2008)

[6] Chen, X., Surani, F. B., Kong, X., Punyamurtula, V. K., and Qiao, Y. Energy absorption performance of steel tubes enhanced by a nanoporous material functionalized liquid. *Applied Physics Letters*, **89**(24), 241918 (2006)

[7] El-Mir, L., Kraiem, S., Bengagi, M., Elaloui, E., Ouederni, A., and Alaya, S. Synthesis and characterization of electrical conducting nanoporous carbon structures. *Physica B*: *Condensed Matter*, **395**(1), 104–110 (2007)

[8] Kucheyev, S. O., Hayes, J. R., Biener, J., Huser, T., Talley, C. E., and Hamza, A. V. Surface-enhanced Raman scattering on nanoporous Au. *Applied Physics Letters*, **89**(5), 53102 (2006)

[9] Biener, J., Wittstock, A., Zepeda-Ruiz, L. A., Biener, M. M., Zielasek, V., Kramer, D., Viswanath, R. N., Weissmüller, J., Bäumer, M., and Hamza, A. Z. Surface-chemistry-driven actuation in nanoporous gold. *Nature Materials*, **8**(1), 47–51 (2008)

[10] Biener, J., Hodge, A. M., Hamza, A. V., Hsiung, L. M., and Satcher, J. H., Jr. Nanoporous Au: a high yield strength material. *Journal of Applied Physics*, **97**(2), 24301 (2005)

[11] Biener, J., Hodge, A. M., Hayes, J. R., Volkert C. A., Zepeda-Ruiz, L. A., Hamza, A. V., and Abraham, F. F. Size effects on the mechanical behavior of nanoporous Au. *Nano Letters*, **6**(10), 2379–2382 (2006)

[12] Hodge, A. M., Biener, J., Hayes, J. R., Bythrow, P. M., Volkert, C. A., and Hamza, A. V. Scaling equation for yield strength of nanoporous open-cell foams. *Acta Materialia*, **55**(4), 1343–1349 (2007)

[13] Fan, H. L. and Fang, D. N. Enhancement of mechanical properties of hollow-strut foams: analysis. *Materials and Design*, **30**(5), 1659–1666 (2009)

[14] Weissmüller, J., Duan, H., and Farkas, D. Deformation of solids with nanoscale pores by the action of capillary forces. *Acta Materialia*, **58**(1), 1–13 (2010)

[15] Gurtin, M. E. and Murdoch, A. I. A continuum theory of elastic material surfaces. *Archive for Rational Mechanics and Analysis*, **57**(4), 291–323 (1975)

[16] Wang, J. X., Huang, Z. P., Duan, H. L., Yu, S. W., Feng, X. Q., Wang, G. F., Zhang, W. X., and Wang, T. J. Surface stress effect in mechanics of nanostructured materials. *Acta Mechanica Solida Sinica*, **24**(1), 52–82 (2011)

[17] Feng, X. Q., Xia, R., Li, X. D., and Li, B. Surface effects on the elastic modulus of nanoporous materials. *Applied Physics Letters*, **94**(1), 011916 (2009)

[18] Lu, Z. X., Zhang, C. G., Liu, Q., and Yang, Z. X. Surface effects on the mechanical properties of nanoporous materials. *Journal of Physics D*: *Applied Physics*, **44**(39), 395404 (2011)

[19] Xia, R., Li, X., Qin, Q., Liu, J., and Feng, X. Q. Surface effects on the mechanical properties of nanoporous materials. *Nanotechnology*, **22**(26), 265714 (2011)

[20] Goudarzi, T., Avazmohammadi, R., and Naghdabadi, R. Surface energy effects on the yield strength of nanoporous materials containing nanoscale cylindrical voids. *Mechanics of Materials*, **42**(9), 852–862 (2010)

[21] Moshtaghin, A. F., Naghdabadi, R., and Asghari, M. Effects of surface residual stress and surface elasticity on the overall yield surfaces of nanoporous materials with cylindrical nanovoids. *Mechanics of Materials*, **51**, 74–87 (2012)

[22] Chen, X., Zhang, S., Dikin, D. A., Ding, W., and Ruoff, R. S. Mechanics of a carbon nanocoil. *Nano Letters*, **3**(9), 1299–1304 (2003)

[23] Mao, S., Han, X. D., Wu, M. H., Zhang, Z., Hao, F., Liu, D. M., Zhang, Y. F., and Hou, B. F. Effect of cyclic loading on apparent Young's modulus and critical stress in nano-subgrained superelastic NiTi shape memory alloys. *Materials Transactions*, **47**(3), 735–741 (2006)

[24] Gao, P. X., Mai, W., and Wang, Z. L. Superelasticity and nanofracture mechanics of ZnO nanohelices. *Nano Letters*, **6**(11), 2536–2543 (2006)

[25] Liu, J. L., Mei, Y., Xia, R., and Zhu, W. L. Large displacement of a static bending nanowire with surface effects. *Physica E*: *Low-Dimensional Systems and Nanostructures*, **44**(10), 2050–2055 (2012)

[26] Wang, G. and Yang, F. Postbuckling analysis of nanowires with surface effects. *Journal of Applied Physics*, **109**(6), 63535 (2011)

[27] Wang, J. S., Wang, G. F., Feng, X. Q., and Qin, Q. H. Surface effects on the superelasticity of nanohelices. *Journal of Physics*: *Condensed Matter*, **24**(26), 265303 (2012)

[28] Dubbeldam, D., Beerdsen, E., Calero, S., and Smit, B. Dynamically corrected transition state theory calculations of self-diffusion in anisotropic nanoporous materials. *The Journal of Physical Chemistry B*, **110**(7), 3164–3172 (2006)

[29] Lu, Z., Huang, J., and Chen, X. Analysis and simulation of high strain compression of anisotropic open-cell elastic foams. *Science China Technological Sciences*, **53**(3), 863–869 (2010)

[30] Lu, Z., Liu, Q., and Chen, X. Analysis and simulation for the tensile behavior of anisotropic open-cell elastic foams. *Applied Mathematics and Mechanics* (*English Edition*), **35**(11), 1437–1446 (2014) DOI 10.1007/s10483-014-1874-7

[31] Cammarata, R. C. Surface and interface stress effects on interfacial and nanostructured materials. *Materials Science and Engineering*: *A*, **237**(2), 180–184 (1997)

[32] Gurtin, M. E., Weissmüller, J., and Larche, F. A general theory of curved deformable interfaces in solids at equilibrium. *Philosophical Magazine A*, **78**(5), 1093–1109 (1998)

[33] Chen, T., Chiu, M., and Weng, C. Derivation of the generalized Young-Laplace equation of curved interfaces in nanoscaled solids. *Journal of Applied Physics*, **100**(7), 74308 (2006)

[34] He, J. and Lilley, C. M. Surface effect on the elastic behavior of static bending nanowires. *Nano Letters*, **8**(7), 1798–1802 (2008)

[35] Wang, G. and Feng, X. Effects of surface elasticity and residual surface tension on the natural frequency of microbeams. *Applied Physics Letters*, **90**(23), 231904 (2007)

[36] Zhu, H. X., Mills, N. J., and Knott, J. F. Analysis of the high strain compression of open-cell foams. *Journal of the Mechanics and Physics of Solids*, **45**(11), 1875–1904 (1997)

[37] Lu, Z., Zhang, J., and Wang, S. Investigation into elastic properties of anisotropic random foam model (in Chinese). *Journal of Beijing University of Aeronautics and Astronautics*, **32**, 1468–1471 (2006)